VIII International Conference on Fracture Mechanics of Concrete and Concrete Structures
FraMCoS-8
J.G.M. Van Mier, G. Ruiz, C. Andrade, R.C. Yu and X.X. Zhang (Eds)

COMPETITION AND INTERPLAY BETWEEN DIFFERENT FAILURE MECHANISMS IN CONCRETE BEAMS STRENGTHENED BY FRP PLATES

M. CORRADO[*], P. CORNETTI[*] AND A. CARPINTERI[*]

[*] Politecnico di Torino
Department of Structural, Geotechnical and Building Engineering
Corso Duca degli Abruzzi 24, 10129 Torino, Italy
e-mail: mauro.corrado@polito.it – pietro.cornetti@polito.it – alberto.carpinteri@polito.it

Key words: Cohesive Model, Fracture Mechanics, FRP, IC-Debonding, PE-Debonding.

Abstract: In the present paper we analyze the competition between different failure mechanisms in fiber reinforced polymer (FRP) strengthened beams. Attention is focused on a three-point bending test of a concrete specimen reinforced by a FRP strip at the bottom. We analyze the competition between the growth of a flexural crack in the concrete beam along its mid-span cross section and the growth of a debonding crack along the concrete-FRP interface starting from the mid-span. This latter phenomenon is usually referred to in the literature as intermediate crack-induced debonding (IC-debonding). For what concerns the IC-debonding, the crack growth is described by an analytical approach based on Linear Elastic Fracture Mechanics (LEFM). This choice corresponds to assume an interface between FRP and concrete with an elastic-perfectly brittle behavior and is justified by the brittleness of the debonding phenomenon. On the other hand, the flexural crack is modeled numerically by means of a cohesive crack, since the cohesive zone model is believed to be more effective to describe crack propagation in the cementitious matrix. The two failure mechanisms are connected since the force in the FRP reinforcement tends to avoid the opening of the flexural crack and, vice-versa, the presence of the flexural crack induces a force increment in the FRP strip that can cause the delamination. Furthermore, the model is also extended to take the concrete crushing failure into account by means of the overlapping crack model, recently developed to describe this failure mode in reinforced concrete beams. The competition and interplay between the different failure modes, as well as the effect of the relevant parameters on the structural behavior, are analyzed in terms of load-displacement curve.

1 INTRODUCTION

Structural rehabilitation is required whenever design mistakes, executive defects or unexpected loading conditions are assessed. Retrofitting techniques may be required in order either to increase the load carrying capacity of the structure, or to reduce its deformations. Among the different rehabilitation strategies, bonding of FRP strips is becoming more and more popular, especially for what concerns concrete structures [1]. The advantages of this technique are several. FRP strips are versatile, easy to install and cause a minimum increase in dimension; furthermore, they have a high strength, a light weight and a long durability.

The structural behavior of FRP-strengthened members is substantially different from that of the original unstrengthened structures and, even more important, new failure modes may occur. Generally speaking, we can list six different failure mechanisms: concrete cover separation, Plate End (PE) debonding, Intermediate Crack

(IC) induced debonding, beam failure due to a critical diagonal (shear) crack (CDC), concrete crushing at the extrados, FRP rupture.

Among the various failure modes observed, a special interest has been recently devoted to the PE debonding of the FRP because of its brittle and catastrophic features, the propagation of the interfacial crack being highly unstable. It is worth noting that PE-debonding of the reinforcement strip is a failure mechanism that may occur both in concrete as well as in metallic FRP-strengthened beams. On the other hand, concrete beams may fail because of an interfacial crack in its turn induced by a flexural crack inside the concrete member. This failure mechanism is named IC-debonding and is characterized by an interfacial crack running toward the edge, i.e. in the opposite direction with respect to what happens in the PE-debonding failure mechanism.

For what concerns the PE-debonding, several models have been proposed to evaluate the interfacial stresses at the edge of the FRP plate. An accurate review of these models can be found in [2]. However, because of the brittleness of the debonding process, an energy approach seems to be more effective. In this respect, Linear Elastic Fracture Mechanics (LEFM) has been applied to analyze PE-debonding by Rabinovitch [3] and, more recently, by Carpinteri et al. [4,5], where the rising of snap-back and snap-through instabilities according to test control have been highlighted.

In order to take into account also the IC-debonding, the model was later extended [6] by applying LEFM to a retrofitted beam where, for the sake of simplicity, the concrete cross section is completely cracked. Although in practical cases this situation is never met, at least before loading, it is worth observing that in laboratory tests sometimes a fully cracked three-point bending (TPB) beam is used [7].

The aim of the present paper is twofold. Firstly, to extend the result presented in Carpinteri et al. [4-6] for an arbitrary value of the relative flexural crack depth, whose value strongly affects the IC-debonding load. Then to couple this model with a detailed analysis of the central beam segment based on the cohesive [8] and overlapping [9] crack models. This analysis allows detecting the growth of the flexural crack and its interplay with the propagation of the IC-debonding crack. Furthermore, the overlapping crack model provides also the conditions for describing the occurrence of concrete crushing at the beam extrados. The competition and interplay between the different failure modes, as well as the effect of the relevant parameters on the structural behavior, are finally analyzed in terms of load-displacement curve.

2 ANALYTICAL MODEL FOR IC- AND PE-DEBONDING

Let us refer to a beam with a rectangular cross section (Fig. 1), in a TPB configuration. The beam span is $2l$ and P is the concentrated load. If z is the axial coordinate with origin at the beam mid-span, in the left side of the beam the bending moment is $M = -P(l-z)/2$.

In the following, the quantities with subscript b refer to the beam to be strengthened and the quantities with subscript r to the reinforcement. Thus E_b, h_b, t_b and E_r, h_r, t_r are the Young modulus, height (or thickness) and width of the beam and of the reinforcement, respectively. As outlined in the introduction, we want to develop a model able to analyze the competition between the flexural crack in the concrete beam and the interfacial cracks between FRP and concrete, either from the mid-span or from the supports. To this aim we firstly consider a given geometry, i.e. we fix all the crack depths: a is the flexural crack length while z_i and z_r are the interfacial crack tips positions (Fig. 1).

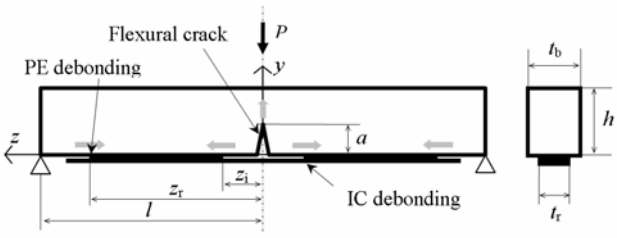

Figure 1: FRP reinforced beam with a rectangular cross section under TPB load. The grey arrows indicate the crack growth directions.

We introduce the following dimensionless parameters: the relative crack depth α, the shear slenderness λ, the mechanical percentage of the reinforcement ρ, the dimensionless longitudinal coordinate $\zeta_i<\zeta<\zeta_r$. In formulae:

$$\alpha = \frac{a}{h_b}\ ,\ \lambda = \frac{l}{h_b},$$

$$\rho = \frac{E_r h_r t_r}{E_b h_b t_b},\ \zeta_i = \frac{z_i}{l},\ \zeta_r = \frac{z_r}{l} \tag{1}$$

Two are the basic assumptions of the subsequent structural analysis. The first is that we assume planar cross sections inside the beam to be strengthened. The second is that the interface between the beam and the reinforcement is modeled as a weak interface, i.e. a bed of linear elastic springs. This is a common assumption in composite material modeling in general and in structural retrofitting in particular. More in details, for the geometry under consideration, peeling stresses are usually negligible. Hence the interface is modeled as a bed of horizontal springs of stiffness k, i.e. $\tau = k\,\delta$, where τ and δ are the shear stress and the relative longitudinal displacement across the interface.

The stress-strain field in the unreinforced cross section ($z_r<z<l$) and in the debonded region ($0<z<z_i$) can be obtained by the simple beam theory. On the other hand, a more accurate analysis is needed in the reinforced portion ($z_i<z<z_r$), where the following three equilibrium equations hold:

$$\int_0^{h_b} \sigma_b\, t_b\, \mathrm{d}y + \sigma_r\, t_r\, h_r = 0,$$

$$\int_0^{h_b} \sigma_b\, y\, t_b\, \mathrm{d}y = M\ ,\ h_r \frac{\mathrm{d}\sigma_r}{\mathrm{d}z} + \tau = 0 \tag{2}$$

where σ_b and σ_r are the normal stresses in the beam and the reinforcement, respectively. The first two equations state the equivalence of the stress distribution with the axial force (which is equal to zero) and with the bending moment M, whereas the third one represents the differential equilibrium of the reinforcement along z. Note that, because of thinness of the FRP plate, we considered the reinforcement as concentrated on the x-axis.

Coupling the equilibrium equations (2) with the assumption of planar cross sections, it is possible to obtain a unique differential equation in the relative longitudinal displacement across the interface, δ [5]:

$$\frac{\mathrm{d}^2\delta}{\mathrm{d}z^2} - \frac{k(1+4\rho)}{E_r h_r}\delta = -\frac{3P}{E_b t_b h_b^2} \tag{3}$$

the relative displacement being related to the strain ε_r in the FRP by the following relationship:

$$\varepsilon_r = \frac{1}{1+4\rho}\left[\frac{3P(l-z)}{t_b h_b^2 E_b} - \frac{\mathrm{d}\delta}{\mathrm{d}z}\right] \tag{4}$$

In order to find the solution to the differential equation (3), we have to impose the proper boundary conditions. At the FRP edge, the stress must vanish and, consequently, $\varepsilon_r = 0$. From Eq. (4), it follows:

$$\left.\frac{\mathrm{d}\delta}{\mathrm{d}z}\right|_{z=z_r} = \frac{3Pl}{E_b t_b h_b^2}(1-\zeta_r) \tag{5}$$

The stress at the other edge ($z = z_i$) of the bonded region can be evaluated approximately by assuming planar cross section in the cracked region at the beam mid-span. Classical beam theory and some analytical manipulations allow to compute the force FFRP in the FRP in the $0<z<z_i$ interval as:

$$F_{FRP} = \frac{3P\rho\lambda}{g(\alpha,\rho)} \tag{6}$$

with:

$$g(\alpha,\rho) = \frac{(1-\alpha)^3 + 4\rho(1+\alpha+\alpha^2)}{1+\alpha} \tag{7}$$

By means of Eqs. (4) and (6), the second boundary condition reads:

$$\left.\frac{\mathrm{d}\delta}{\mathrm{d}z}\right|_{z=z_i} = \frac{3Pl}{E_b t_b h_b^2} f(\zeta_i,\alpha,\rho) \tag{8}$$

with:

$$f(\zeta_i,\alpha,\rho) = (1-\zeta_i) - \frac{1+4\rho}{g(\alpha,\rho)} \tag{9}$$

Equation (3) can now be solved, providing the relative displacement field δ and the

related shear stress field $\tau=k\delta$ along the interface. The solution is plotted in Fig. 2. It is evident that at both the edges of the bonded zone a stress concentration, responsible of the delamination, appears. Since delamination is a remarkably brittle phenomenon, a failure criterion based on LEFM can be exploited to address the problem. To this aim, we need to evaluate the strain energy release rate, which, in the case of a weak interface, is directly related to the shear stress τ_{max} at the crack tip by the relationship [5]:

$$\mathcal{G}=\frac{\tau_{\max}^2}{2k} \tag{10}$$

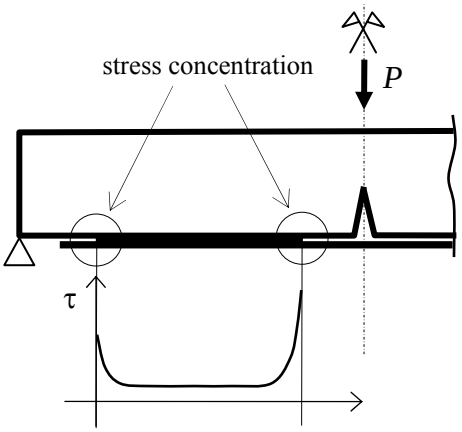

Figure 2: Shear stress concentrations at the edges of the bonded region.

According to LEFM, edge debonding will occur when the strain energy release rate reaches the interfacial fracture energy $\mathcal{G}_{iF}$. In the case of IC-debonding, τ_{max} is given by $\tau(\zeta_i)$ and, correspondingly, the force in the FRP is equal to:

$$\left(F_{\mathrm{FRP}}\right)_{\mathrm{IC}}= \tag{11}$$
$$=\frac{\sqrt{2\rho\left(1+4\rho\right)}}{g\left(\alpha,\rho\right)f_{\mathrm{IC}}\left(\alpha,\beta,\rho,\zeta_{\mathrm{i}},\zeta_{\mathrm{r}}\right)}\sqrt{\mathcal{G}_{\mathrm{iF}}E_{\mathrm{b}}t_{\mathrm{b}}h_{\mathrm{b}}}$$

where:

$$f_{\mathrm{IC}}\left(\alpha,\beta,\rho,\zeta_{\mathrm{i}},\zeta_{\mathrm{r}}\right)= \tag{12}$$
$$=\frac{1}{\beta}+\frac{1-\zeta_{\mathrm{r}}}{\sinh\left[\beta\left(\zeta_{\mathrm{r}}-\zeta_{\mathrm{i}}\right)\right]}-\frac{f\left(\alpha,\rho,\zeta_i\right)}{\tanh\left[\beta\left(\zeta_{\mathrm{r}}-\zeta_{\mathrm{i}}\right)\right]}$$

and β is a dimensionless parameter:

$$\beta=l\sqrt{\frac{E_{\mathrm{r}}h_{\mathrm{r}}}{k\left(1+4\rho\right)}} \tag{13}$$

In a similar way, it is possible to derive the load causing PE debonding, which will occur when τ_{max} is given by $\tau(\zeta_r)$.

Eq. (11) represents the critical condition for the growing of the delamination crack. We need now to determine the load causing the growth of the flexural crack. To accomplish this task, in the next section we will couple the present analytical model with a cohesive crack model (CCM) [8] description of the flexural crack occurring at the mid-span. The choice of using, for the flexural crack, the CCM instead of a LEFM framework is due to the following observations: fracture inside the concrete is typically quasi-brittle and CCM is able to detect crack initiation. Furthermore, the CCM has been recently extended to describe also concrete crushing failures [10], so that a further failure mode can be caught by the present analysis.

In order to decide which crack will propagate at a given step of the loading process, the CCM needs not only the critical load (11) but also the relationship between the crack mouth opening and the force in the reinforcement, which will enter the algorithm as a constitutive law. The crack mouth opening is equal to twice the relative displacement $\delta(0)$ evaluated at the mid-span. Within the assumption previously provided, the desired relation is given by:

$$\delta\left(0\right)=\frac{l}{E_{\mathrm{r}}t_{\mathrm{r}}h_{\mathrm{r}}}\zeta_{\mathrm{i}} \tag{14}$$
$$\left[1+4\rho-g\left(\alpha,\rho\right)\left(1-\frac{\zeta_{\mathrm{i}}}{2}\right)\right]F_{\mathrm{FRP}}$$

where for the sake of simplicity we neglect the interface compliance, since its contribution is negligible with respect to the other terms. The relative displacement $\delta(0)$ is thus given by the different elongation of the reinforcement with respect to the beam intrados.

Similarly, the mid-span deflection $v(0)$ can be evaluated as:

$$v(0)=\frac{2Pl^3}{E_b t_b h_b^3}\left\{(1-\zeta_r)^3+\right. \tag{15}$$
$$+\frac{1+\rho}{1+4\rho}(\zeta_r-\zeta_i)(3-3\zeta_i-3\zeta_r+\zeta_i^2+\zeta_i\zeta_r)+$$
$$\left.+\zeta_i\left[\zeta_i^2-3\left(1-\frac{3\rho}{2g(\alpha,\rho)}\right)\zeta_i+3\left(1-\frac{3\rho}{g(\alpha,\rho)}\right)\right]\right\}+$$
$$+\varphi(0)l$$

where the three terms in curly brackets represent the contributions of the unreinforced portion, of the reinforced-bonded region and of the reinforced-debonded part of the beam, respectively. The term $\varphi(0)\times l$ represents the contribution of the localized rotation at the beam mid-span due to the presence of the flexural crack. Within the present analysis, it is equal to $\delta(0)\times\lambda$. However, it is easily argued that its actual value is largely underestimated by the present analysis, since it completely disregards the process zone occurring at the tip of the flexural crack. Therefore, we will evaluate such a contribution by means of a cohesive crack model description of the central portion of the beam, as explained in the next section.

3 NUMERICAL FORMULATION FOR THE INTERACTION BETWEEN DEBONDING AND FLEXURAL CRACK

The numerical algorithm proposed by Carpinteri et al. [10] for the analysis of reinforced concrete beams in bending is herein extended to concrete beams strengthened by means of FRP strips. In particular, the evaluation of the load carrying capacity is performed by analyzing only the central portion of the beam, having a span to depth ratio equal to unity. Such an element, shown in Fig. 3a, is subjected to a constant bending moment, M, function of the applied force on the basis of the structural and the loading systems. The main mechanical nonlinearities are taken into account, namely, the tensile crack propagation, the concrete crushing in compression, and the FRP debonding, on the basis of the analysis presented in the previous section.

The flexural crack propagation is modeled by means of the well established CCM [8]. A simple linear softening function is herein considered, although bi-linear or even more complicated relationships may be assumed depending on the characteristics of the considered material and the analyzed problem. The critical value of the crack opening displacement, beyond which the cohesive stresses vanish, and the fracture energy, GF, are assumed as material properties.

As far as modeling of concrete crushing failure is concerned, the overlapping crack model (OCM) [9] is adopted. According to such an approach, that is the analogous of the CCM for compression, the inelastic and localized deformation in the post-peak regime is described by a fictitious interpenetration of the material, while the remaining part of the specimen undergoes an elastic unloading. As a result, a stress-displacement (overlapping) relationship describes how the stress in the damaged material decreases from its maximum value as the fictitious interpenetration increases. The crushing energy, $\mathcal{G}_C$, which is a dissipated surface energy, is defined as the area below the softening curve. It is assumed as a material property, since it is only slightly affected by the structural size, as shown in [9], where an extended validation of the OCM for concrete-like materials has been proposed in the case of specimens with different slendernesses and/or sizes.

The numerical algorithm is based on a discrete form of the elastic equations governing the mechanical response of the system. The concrete member is considered as constituted by two symmetrical sub-elements characterized by an elastic behavior, connected by means of (n) pairs of nodes (Fig. 3a). In this approach, all the mechanical nonlinearities are localized in the mid-span cross section, where cohesive and overlapping stresses are replaced by equivalent nodal forces, F_i, by integrating the corresponding stresses over the nodal spacing. The FRP bridging contribution is modeled by means of an external force, FFRP, applied on the crack mouth (at the level of the first node). The depths of the adhesive layer and of the FRP strip are assumed as negligible, compared to the beam height, h_b. With

reference to Fig. 3a, the horizontal forces, F_i, acting at the i-th node along the mid-span cross-section can be computed as follows:

$$\{F\} = [K_w]\{w\} + \{K_M\} M \tag{16}$$

where: $\{F\}$ is the vector of nodal forces, $[K_w]$ is the matrix of the coefficients of influence for the nodal displacements, $\{w\}$ is the vector of nodal displacements, $\{K_M\}$ is the vector of the coefficients of influence for the applied moment M.

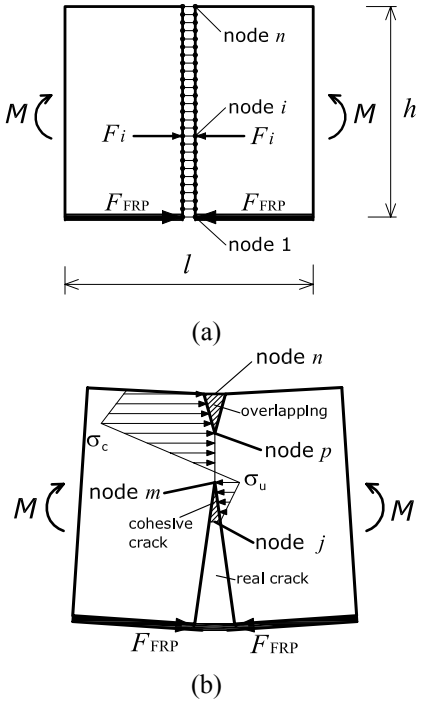

Figure 3: Finite element nodes (a) and force distribution (b) along the symmetry cross-section.

Equation (16) constitutes a linear algebraic system of (n) equations and ($2n$+1) unknowns, $\{F\}$, $\{w\}$ and M. With reference to the generic situation reported in Fig. 3b, (n) additional equations can be introduced by considering the constitutive laws for concrete in tension and compression and for the FRP strip (Eq. (14)). It is worth noting that the reaction in the FRP strip is a function of the bond length and the flexural crack depth in addition to the crack opening, making possible to accurately evaluate the competition between the different failure modes. At each step, in fact, the load carrying capacity is determined by one of the four possible critical conditions: flexural crack propagation, crushing zone advancement, IC debonding, and PE debonding. The condition to which corresponds the minimum value for the applied load is that assumed as the critical one for the considered step of calculation. Therefore, the driving parameters are the cracking and crushing extensions as well as the debonding lengths, that are updated step-by-step. In particular, the cohesive and crushing crack tips are moved to the next node, whereas the debonding lengths are increased by a prefixed quantity. Finally, at each step of calculation the localized rotation due to the presence of flexural cracking and crushing, $\varphi(0)$ in Eq. (15), is obtained by subtracting the elastic contribution from the rotation of the beam portion. The latter one is computed by means of elastic coefficients of influence, that, along with those in Eq. (16), have to be computed a priori using a finite element analysis:

$$\varphi(0) = \{D_w\}^T \{w\} + D_M M \tag{17}$$

4 NUMERICAL RESULTS

4.1 Competition between IC-debonding and flexural crack propagation

The behavior of FRP-strengthened beams subjected to TPB test is herein analyzed by means of the new proposed algorithm. In the following, the relative crack depth, α, entering Eqs. (6)-(15) is given by the position of the fictitious crack tip, and therefore, it is equivalent to the sum of the real and the fictitious crack lengths. The width and the height of the beam are assumed equal to 100 and 200 mm, respectively, for all the numerical simulations, as well as the FRP strip width is fixed to 100 mm. The FRP and concrete Young moduli are equal to 210,000 MPa and 30,000 MPa, respectively.

A comparison with the results of the former analytical model presented in [6], which assumes α=1 since the beginning of the loading process, is shown in Fig. 4 in terms of load vs. mid-span deflection, for ρ=0.070, $\mathcal{G}_{iF}$=0.065 N/mm, and σ_c=25 MPa. The new

proposed model (thick curve) permits to capture the decrease in the stiffness of the ascending branch due to the cohesive crack propagation. On the contrary, the analytical model (thin curve) neglects such a contribution. Both the models predict a load increase up to the onset of the IC-debonding, although the interaction between flexural crack and FRP debonding leads to a slight reduction in the maximum bearing load, P_{max}. This interaction is also evident in the post-peak branch, where several local instabilities are obtained due to flexural crack propagations. In this case, the extension of the crushing zone is limited and it does not influence the overall response. Therefore, the area enclosed by the thick curve is equal to that of the thin curve (energy dissipated by the FRP debonding) plus that of the dashed curve (energy dissipated by the flexural crack), which refers to the unreinforced beam.

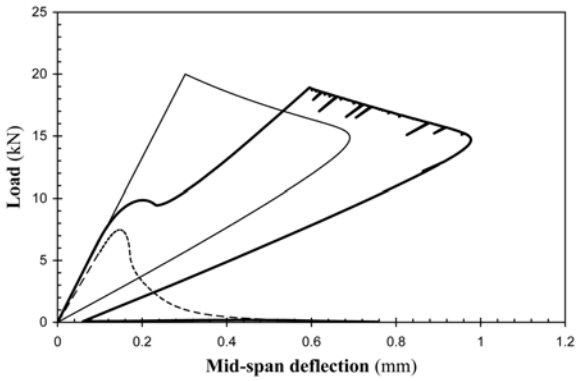

Figure 4: Comparison between the former model (thin line) and the present model (thick line). The dashed curve refers to the unstrengthened beam.

The effects of the reinforcement amount are analyzed in Fig. 5, where different mechanical percentages, ρ, are considered varying from zero up to 0.140. The increase in the FRP amount determines an increase in the stiffness of the ascending branch. Such a stiffening is more evident after the cracking load, i.e., when the real crack propagation occurs. The maximum load is an increasing function of the FRP amount, whereas the cracking load is almost constant. In particular, for $\rho \leq 0.018$ the phenomenon of hyper-strength is obtained. The post-peak behavior becomes more and more brittle by increasing the reinforcement percentage, with a considerable decrease in the anelastic displacement. All the cases shown in Fig. 5 are characterized by IC-debonding failure mechanism, with limited concrete crushing effect.

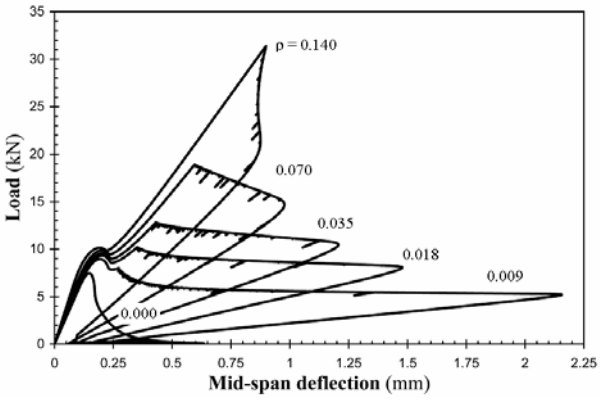

Figure 5: Load vs. mid-span deflection curves for different mechanical percentages of reinforcement. All the curves refer to IC-debonding failure mechanism.

According to the present model, the maximum load carrying capacity, P_{max}, is function of the relative flexural crack length, α, that, in turn, depends on the FRP amount and the concrete compressive strength. The ratio between the maximum load predicted by the proposed model and that given by the previous analytical model, which assumes $\alpha=1$, is shown in Fig. 6 as a function of the mechanical percentage of reinforcement. It results to be a decreasing function of the FRP amount, and, in particular, it is greater than unity for $\rho<0.04$. Such a trend can be explained by analyzing the variation of the FRP debonding strength as a function of the flexural crack length, α, shown in Fig. 7. The peak load of the curves in Fig. 5 corresponds to the onset of the FRP delamination, that, typically, takes place for α equal to 0.7 about. In the case of small amount of reinforcement, such as $\rho=0.018$, the delamination force is a monotonic decreasing function of the relative crack depth, and, therefore, the force referred to $\alpha=1.0$ is lower than that referred to $\alpha=0.7$. Furthermore, the cohesive stress distribution along the process zone has a significant

contribution on the load carrying capacity with respect to the case of completely cracked cross section. By increasing the reinforcement amount, the diagrams of the delamination force vs. relative crack depth presents a minimum for α around 0.7 (see the curve referred to ρ=0.140 in Fig. 7). In this case, the peak load given by the proposed model is lower than that relative to α=1.0.

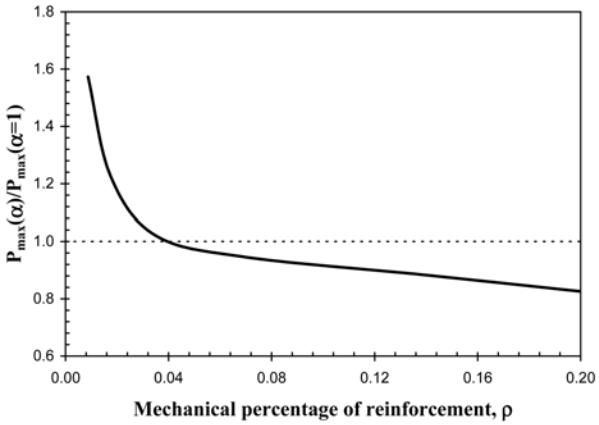

Figure 6: Effect of the flexural crack length, α, on the load carrying capacity.

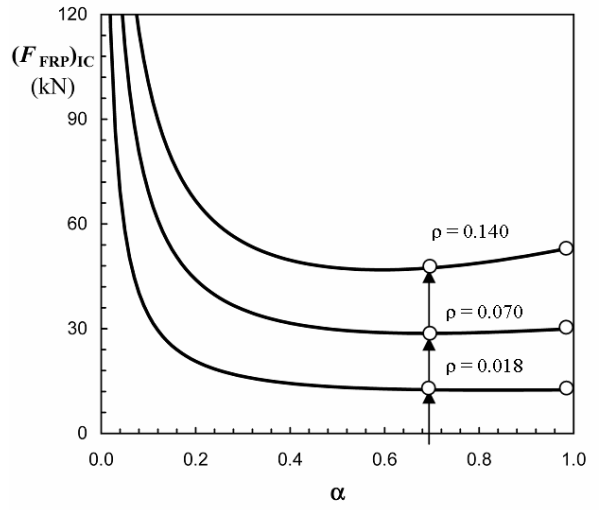

Figure 7: Effect of the flexural crack length, α, on the FRP strip reaction.

4.2 Transition between different failure mechanisms

The transition between the three different failure mechanisms analyzed by the proposed approach, namely PE-debonding, IC-debonding and crushing, is governed by the mechanical and geometrical parameters of the beams. With reference to the beam considered in the previous section, a transition from IC-debonding to crushing failure is obtained when the mechanical reinforcement percentage reaches the value 0.350, as shown in Fig. 8a. In this case, the crushing zone becomes wider and wider by approaching the maximum load, that, in any case, is determined by the onset of the IC-debonding. Moreover, at a certain point of the FRP delamination and the concrete crushing processes characterizing the post-peak regime, the equilibrium along the mid-span cross section is no longer verified. This phenomenon may be associate to a global collapse due to concrete crushing.

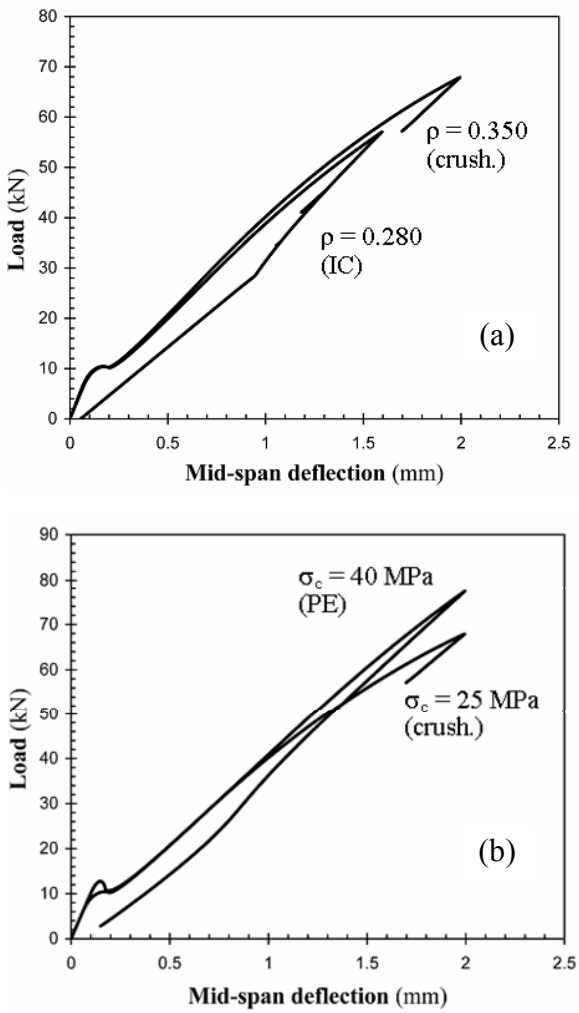

Figure 8: Load vs. mid-span deflection curves: transition from IC-debonding to crushing failure by increasing the mechanical percentage of reinforcement (a); transition from crushing to PE-debonding failure by increasing the concrete compressive strength (b).

On the other hand, a transition from crushing to PE-debonding failure is obtained by increasing the concrete compressive strength from 25 MPa to 40 MPa, for a constant value of the reinforcement amount, ρ=0.350 (Fig. 8b). In this case, the peak load is determined by the onset of the PE-debonding. Compared to the case of crushing failure, the overall stiffness is constant up to the peak load (expect for the initial tension-stiffening effect), due to a limited damage of the concrete in compression. Finally, it is worth noting that, even if the curves shown in Fig. 8 have been obtained by assuming very high reinforcement amounts, maybe far from reality, similar behaviors can be obtained, in a realistic way, by increasing the fracture energy of the interface.

The complex competition between the three different failure mechanisms has been studied by means of a parametric analysis, and summarized in the interaction diagrams shown in Figs. 9-12. The investigated parameters are: mechanical percentage of reinforcement ρ, relative reinforcement length ζ_r, beam slenderness λ, concrete compressive strength σ_c, and fracture energy of the interface $\mathcal{G}_{iF}$. All the other parameters –beam width and height, elastic moduli of concrete and FRP– are kept constant, equal to those assumed in the previous section. The diagram in Fig. 9 refers to λ=6, σ_c=30 MPa, and $\mathcal{G}_{iF}$=0.08 N/mm. It is clear that IC-debonding failure is the most frequent for real cases, characterized by small reinforcement amounts and relative bonding lengths around 0.8. PE-debonding failure takes place in the case of small reinforcement lengths and/or high reinforcement percentages, whereas crushing failure occurs for high reinforcement lengths (ζ_r>0.65) and percentages (ρ>0.30). In the case of small reinforcement amount, there is a region where the failure mechanism is due to both IC and PE delaminations. In such cases, the maximum load is determined by the onset of IC-debonding, whereas PE-debonding prevails when the residual bond length decreases below a certain value. The effect of the beam slenderness on the transition between the failure mechanisms can be evidenced by comparing the diagram in Fig. 9 with those in Fig. 10. In particular, a decrease in the slenderness from 6 to 3 (Fig. 10a) leads to an enlargement of the region characterized by a strong competition between IC- and PE-debonding and a shrinkage of the region of crushing failure. An opposite behavior is obtained by increasing the slenderness from 6 to 12 (Fig. 10b).

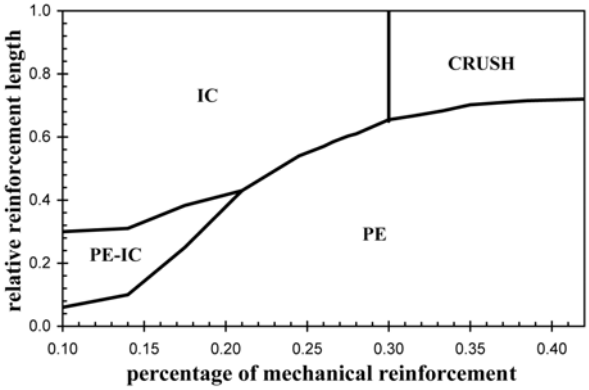

Figure 9: Failure mechanism as a function of geometrical and mechanical parameters for λ=6. σ_c=30 MPa, and $\mathcal{G}_{iF}$=0.08 N/mm.

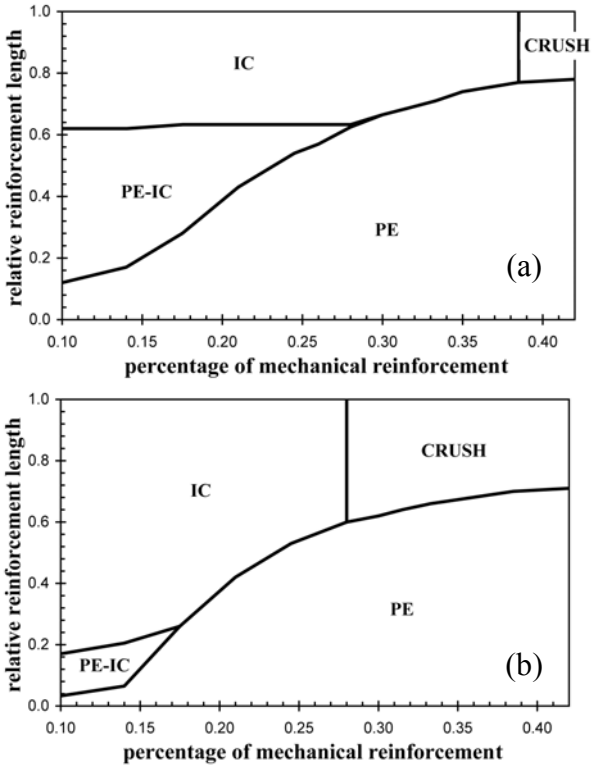

Figure 10: Failure mechanism as a function of geometrical and mechanical parameters for σ_c=30 MPa, $\mathcal{G}_{iF}$=0.08 N/mm and λ=3 (a); and λ=12 (b).

As regards the crushing failure, it mainly depends on the considered concrete grade, as shown in Fig. 11. A decrease in the concrete compressive strength from 30 to 20 MPa determines an enlargement of crushing failure, with the appearance of an interplay between IC-debonding and concrete crushing for an intermediate range of reinforcement amounts. Analogously, the crushing failure is also favoured by the increase in the interface fracture energy, as shown in Fig.12.

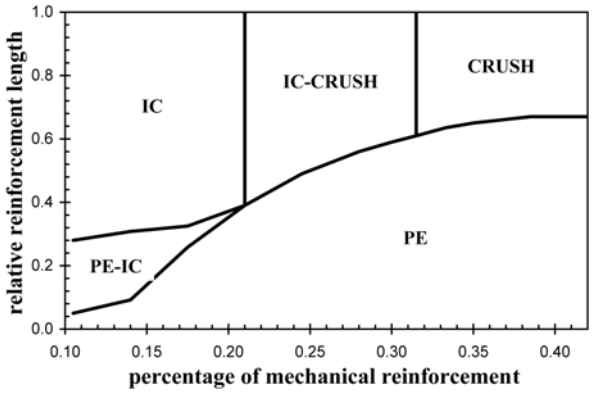

Figure 11: Failure mechanism as a function of geometrical and mechanical parameters for λ=6, σ_c=20 MPa, and $\mathcal{G}_{iF}$=0.08 N/mm.

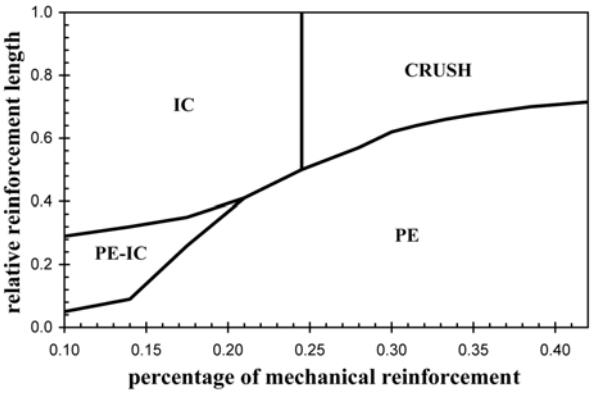

Figure 12: Failure mechanism as a function of geometrical and mechanical parameters for λ=6, σ_c=30 MPa, and $\mathcal{G}_{iF}$=0.12 N/mm.

5 CONCLUSIONS

A coupled analytical/numerical model has been proposed to analyze the interaction between different failure mechanisms characterizing the behavior of FRP-strengthened concrete beams. The main novelty is due to the fact that the actual flexural crack propagation and the damage of concrete in compression occurring along the mid-span cross section during the loading process, as well as their interaction with the FRP delamination modes are taken into account. In particular, both the nonlinear processes characterizing the behavior of concrete in tension and compression are modeled by means of a cohesive zone model. A step-by-step solution updating the cracking and crushing extensions and the debonding lengths, permits all the local instabilities, such as snap-back branches, to be captured without any loss of the loading control.

The tension-stiffening characterizing the increasing branch of the load vs. displacement curves is correctly described by means of the cohesive crack model. As regards the interaction between different failure mechanisms, the flexural collapse has a significant effect on the peak load corresponding to IC-delamination failure, whereas has a limited effect on the PE-debonding failure mode.

The proposed parametric analysis has evidenced that IC-debonding failure mechanism is the most frequent for real cases, usually characterized by high relative reinforcement lengths and low reinforcement amount, whereas crushing failure prevails in the case of low concrete compressive strength, high interface fracture energy, high reinforcement amount and high relative reinforcement length. PE-debonding failure mechanism occurs for low relative reinforcement length and low beam slenderness.

Future developments will regard the extension of the model to concrete beams reinforced by steel bars and strengthened by FRP strips. Such cases, in fact, are the most interesting for practical applications, as well as the most studied from an experimental point of view.

AKNOWLEDGEMENTS

The Authors acknowledge the financial support of the Italian Ministry of Education,

University and Research to the project "Advanced applications of fracture mechanics for the study of integrity and durability of materials and structures" within the PRIN program for the year 2008.

REFERENCES

[1] Oehlers, D.J., Seracino, R., 2004. *Design of FRP and Steel Plated RC Structures.* Elsevier.

[2] Mukhopadhyaya, P., Swamy, N., 2001. Interface shear stress: a new design criterion for plate debonding. *J. Compos. Constr.* **5:**35-43.

[3] Rabinovitch, O., 2004. Fracture-mechanics failure criteria for RC beams strengthened with FRP strips – a simplified approach. *Compos. Struct.* **64**:479-92.

[4] Carpinteri, A., Cornetti, P., and Pugno, N., 2007. Debonding in FRP strengthened beams: stress assessment versus fracture mechanics approach. In Carpinteri et al (eds), *Design, Assessment and Retrofitting of RC Structures; Proc. of the 6th Inter. Conf. on Fract. Mech. of Conc. & Conc. Struct (FraMCoS-6),* June 17-22, 2006**,** Catania, Italy; pp.1053-60.

[5] Carpinteri, A., Cornetti, P., Pugno, N., 2009. Edge debonding in FRP strengthened beams: stress assessment versus fracture mechanics approach. *Eng. Struct.* **31**:2436-47.

[6] Cornetti, P., Puzzi, S., Carpinteri, A., 2007 Failure mechanisms in beams strengthened with adhesive strips. In *Proc. of the XVIII Congr. AIMETA di Meccanica Teorica ed Applicata*, September 11-14, 2007, Brescia, Italy.

[7] Accardi, M., 2004. Strengthening of masonry structural elements subjected to out-of-plane loads using CFRP Reinforcement. *PhD Thesis*, University of Palermo.

[8] Carpinteri, A., 1989. Cusp catastrophe interpretation of fracture instability. *J. Mech. Phys. Solids* **37**:567-82.

[9] Carpinteri, A., Corrado, M. and Paggi, M., 2011. An analytical model based on strain localization for the study of size-scale and slenderness effects in uniaxial compression tests. *Strain* **47**: 351-62.

[10] Carpinteri, A., Corrado, M., Mancini, G. and Paggi, M., 2009. Size-scale effects on plastic rotational capacity of reinforced concrete beams. *ACI Struct. J.* **106**:887-96.